ADAPTIVE CONTROL ALGORITHM FOR SENSORLESS SWITCHED RELUCTANCE MOTOR

Honglin WANG[1*]

Nowadays, sensorless switched reluctance motors are popular due to their unique advantages. However, the current method of controlling switched reluctance motors without position sensors has the problem of low accuracy. To optimize the capability of sensorless switched reluctance motor control, this study suggested an enhanced backpropagation neural network algorithm that combined genetic algorithm, adaptive learning rate algorithm, additional momentum term algorithm, and backpropagation neural network. Moreover, the enhanced algorithm was combined with a proportional integral derivative controller to construct an adaptive proportional integral derivative control system for sensorless switched reluctance motors. The average running time and average accuracy of this method were 0.79 seconds and 97.9%, respectively, which were significantly better than the compared algorithms. In addition, a performance comparison analysis was conducted on the control system based on this method, and it was found that the system outperformed the comparison system in terms of load torque, motor speed response, and rotor angle estimation error. The adaptive control algorithm for sensorless switched reluctance motors proposed in the study has strong robustness, adaptability, and feasibility, which helps to improve the accuracy of sensorless control of switched reluctance motors.

Keywords: SRM; No position sensor; Adaptive; Control; BP; PID

1. Introduction

Currently, the Switched Reluctance Motor (SRM) is popular in industrial applications and the automotive industry due to its simple structure, high efficiency, and energy-saving capabilities [1]. However, the current method of using sensorless control for SRM has a problem of low accuracy [2]. Although many experts have conducted relevant research, the results are still unsatisfactory [3]. Dejamkhooy A and Ahmadpour A proposed an optimization control model to solve the problem of reduced efficiency of SRM in discrete mode under high-speed applications, but the control effect was poor [4]. To address the issue of the excessive number of position sensors in SRM systems, Fang C et al. proposed a current estimation method for SRMs. Although this method showed some effectiveness, the results were not satisfactory [5]. Sun X et al. proposed an improved SRM driver position signal evaluation method to improve the SRM's fault tolerance in intricate settings, which was effective [6]. Meanwhile, Kumar MN and Chidanandappa R proposed a control

* Corresponding author, e-mail: HongL.01Wang@outlook.com
[1] School of Electrical and Information, Zhenjiang College, Zhenjiang, China

algorithm based on particle swarm optimization combined with Proportional Integral Derivative (PID) controller to solve the problem of large torque ripple and inaccurate speed response of SRM. Through the algorithm comparison experiment, the results indicated that this algorithm showed good performance under all load conditions and was superior to the comparison algorithm [7]. Similarly, aiming at the influence of SRM parameter uncertainty on electromagnetic torque, Jing B et al. set up a neural network sliding mode controller based on parametric online learning. Simulation experiments showed that this method could effectively learn SRM parameters, reduce torque ripple, and improve system stability [8].

At present, sensorless SRM uses a PID controller to detect the rotor position, thereby achieving precise control of the Switched Reluctance Motor Drive (SRD) system and improving system reliability, which has become a research hotspot. Back Propagation Neural Network (BP) has the advantages of strong self-learning adaptability, high flexibility, and the ability to automatically extract features, and is widely used in fields such as system control. However, due to the use of gradient descent to correct the weights according to the negative gradient direction of the error function, it has drawbacks related to local minima and lacks a guarantee of convergence. Genetic Algorithm (GA) has advantages such as strong global optimization ability. The additional momentum term algorithm is an improved BP algorithm, which can help the network maintain a certain memory during the learning process, allowing the network to consider previous information when adjusting weights, thereby accelerating convergence speed and reducing the possibility of falling into local minima [9]. The adaptive learning rate algorithm is a strategy for dynamically adjusting the learning rate in real time based on the error changes during network training, effectively improving the adaptive learning ability of the BP algorithm. Many scholars conducted relevant research. For example, Li C et al. proposed a GA-BP method to find the proper parameters for the cladding process, which was effective [10]. In addition, Shen W et al. proposed a BP optimization model with polynomial decay learning rate to handle the limitations of traditional BP. The model improved evaluation accuracy, but the improvement was relatively low [11].

The above research indicates that although the adaptive control methods currently applied to sensorless switched reluctance point sets have some effectiveness, their control accuracy is still relatively low. Therefore, this study combines GA, additional momentum term algorithm, adaptive learning rate algorithm, and BP to construct an improved BP and apply it to PID, thereby constructing an adaptive PID control model for sensorless SRM based on the improved BP. The innovation lies in the combination of GA, additional momentum term algorithm, adaptive learning rate algorithm, and BP, aiming to improve the system operation stability of SRM. It is expected that this method can contribute to enriching the adaptive control theory of sensorless SRM.

2. Methods and Materials

2.1 Construction of the Improved BP Model Integrating Adaptive Learning Rate, Additional Momentum, and GA

The speed regulation of switch magnet group motors is often controlled without position sensors, but their doubly salient structure gives them high nonlinear characteristics, resulting in a decrease in PID control performance [12]. Finding a solution to improve the adaptive control performance of sensorless SRM is significant for enhancing the stability of motor systems [13]. Therefore, this study utilizes the adaptive learning ability of BP to adjust the parameters of PID, and introduces adaptive learning rate, additional momentum method, and GA to improve the shortcomings of BP algorithm. Finally, the improved BP and PID are combined to construct a PID adaptive control system for sensor SRMs based on the improved BP. Before building the system, it is necessary to construct an improved BP. BP neural network is a kind of neural network model that optimizes its own threshold and weights through learning. It has advantages such as strong nonlinear ability and approximation ability and is widely used in fields such as control [14-15]. However, BP is prone to getting stuck in local minima and lacks a guarantee of convergence when using the gradient descent method to adjust weights based on the error function's negative gradient direction. To solve its slow convergence speed defect, adaptive learning rate is introduced to adaptively adjust and optimize it, and the calculation equation is shown in equation (1).

$$\eta(z+1)=\begin{cases}1.05\eta(z) & SSE(z+1)<SSE(z)\\ 0.7\eta(z) & SSE(z+1)>SSE(z-1)\\ \eta(k) & \text{Others}\end{cases} \tag{1}$$

In equation (1), η is the learning rate, SSE is the mean square error; z is the iteration. To make BP avoid the local minimum, the additional momentum algorithm is introduced, and the calculation equation is shown in equation (2).

$$mc=\begin{cases}0 & SSE(z)>SSE(z-1)\cdot a\\ 0.95 & SSE(z)>SSE(z-1)\\ mc & \text{Others}\end{cases} \tag{2}$$

In equation (2), mc is the momentum factor. However, BP suffers from training instability due to its random input of weights and thresholds. The GA demonstrates robust global optimization capabilities, enabling effective optimization of weights and thresholds in BP. Fig. 1 illustrates the fundamental process of the GA [16].

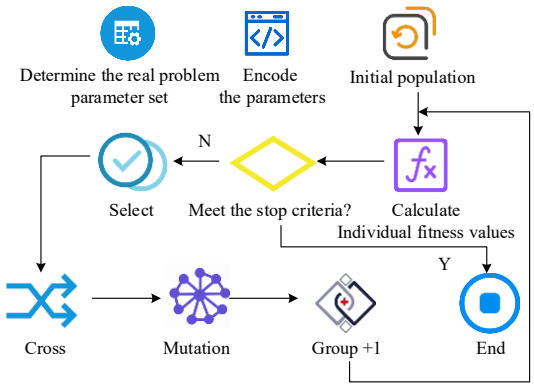

Fig.1 The Basic Flow Chart of GA

In Fig. 1, GA first encodes the parameters using applicable methods such as binary or real numbers and performs initialization operations to randomly generate the initial population. Secondly, the fitness value of each individual is calculated and searched for. Then, the population is evolved and genetically manipulated to generate a new generation of population. Finally, the fitness values of individuals in the population are determined to meet the conditions. If they meet the conditions, the algorithm is terminated. The calculation equation for GA is shown in equation (3).

$$SGA = f(\beta, E, P_0, N, \lambda, H, Q, V) \tag{3}$$

In equation (3), β represents the encoding method of individuals; E represents the evaluation function of individual fitness; P_0 represents the initial population; N represents the population size; λ is the operator; H is the crossover operator; Q is the mutation operator; V represents the termination condition. Based on the above content, the adaptive learning rate algorithm, GA, additional momentum algorithm, and BP are combined to construct an improved BP algorithm, as shown in Fig. 2.

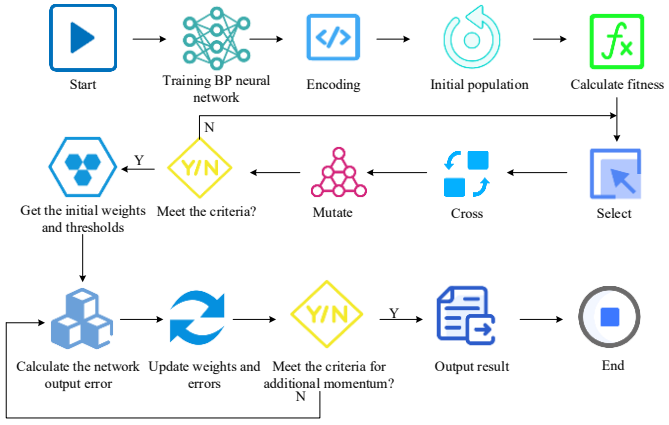

Fig. 2 Improved BP algorithm flow chart

In Fig. 2, the weights and thresholds of BP are encoded with real numbers and randomly selected in the range of 0 to 1 to generate the initial population. Secondly, the population evolves through selection, crossover, and mutation operations, generating a new generation of genes and calculating fitness values for individuals to select the optimal value. The selected optimal value is judged, and if it meets the conditions, the initial weight and threshold for BP are determined by this measure; If not met, the above operations are carried out until the conditions are met. Next, the obtained initial weights and thresholds are used as input values for BP training, and the error value of the network is calculated through forward propagation. Finally, the error values are allocated through BP and updated as new weights and thresholds for the network. In this process, the learning rate of the network is automatically selected using an adaptive learning rate. Finally, whether the value meets the additional momentum criteria and setting conditions is determined. If it does, the result is outputted and the training is ended; If not met, the error is recalculated until the condition is met.

2.2 Design of Adaptive PID Control System for Position sensorless SRM Based on Improved BP

Due to the difficulty of achieving good control effects with traditional sensorless PID control, and the fact that most commonly-used neural network control systems consist of two networks, the system is too complex. Therefore, this study combines an improved BP with traditional PID to construct an adaptive PID controller. Before building an adaptive PID controller, it is necessary to understand the expression of PID, and its classical incremental calculation equation is shown in equation (4).

$$u(c)=u(c-1)+U_p[\tau(c)-\tau(c-1)]+U_I\tau(c)+U_D[\tau(c)-2\tau(c-1)+\tau(c-2)] \quad (4)$$

In equation (4), U_D is the differential coefficient; U_I is the integral coefficient; U_p is the proportional coefficient; τ is the error; u is the optimal control quantity; c is the number of iterations. Therefore, it is substituted into the 3-layer BP to obtain the PID parameter structure controlled by the improved BP, as shown in Fig. 3. In Fig. 3 the three layers of BP correspond their output nodes to the three coefficient parameters of PID control: U_D, U_I, and U_p. ξ is the input value. Since the parameter value cannot be negative, the activation function of the HL and OL are Sigmoid and logarithmic.

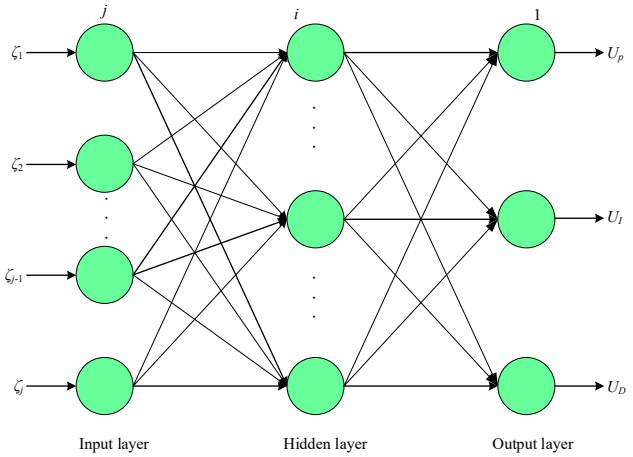

Fig. 3. PID Parameter Structure of Improved BP Control

The improved BP adjusts the PID parameter IL calculation equation as shown in equation (5).

$$O_j^1 = \tau(c-j) \quad (5)$$

In equation (5), ∂_J^1 is the IL control of PID parameters. The calculation equation for the HL control is shown in equation (6).

$$\begin{cases} net_i^2(c) = \sum_{j=0}^{m} w_{ij}^2 \psi_j^1(c) \\ O_l^2(c) = g[net_i^2(c)] \end{cases} \quad (6)$$

In equation (6), net_i^2 is BP; w_{ij}^2 is the weight of HL neurons; ∂_l^2 is the HL control of PID parameters. Equation (7) shows the control calculation equation for the OL.

$$\begin{cases} net_i^3(c) = \sum_{i=0}^{\partial} w_{ij}^3 O_i^2(c) \\ O_l^3(c) = f[net_i^3(c)] \\ O_0^3(c) = u_p \\ O_1^3(c) = u_I \\ O_2^3(c) = u_D \end{cases} \quad (7)$$

In equation (7), w_{ij}^3 is the weight of each neuron in the OL; O_l^3, O_0^3, O_1^3, and O_2^3 are the thresholds of each neuron in the OL, and $l = 0,1,2$. Equation (8) shows the equation for adjusting the weight of the OL.

$$\begin{cases} \Delta w_{li}^3(c+1) = \eta \delta_i^2 O_i^2(c) + \alpha \Delta w_{li}^3(c) \\ \delta_l^3 = \tau(c+1) \cdot \frac{\partial y(c)}{\partial u(k)} \cdot \frac{\partial u(c)}{\partial O_i^3(c)} \cdot f'[net_i^3(c)] \end{cases} \quad (8)$$

In equation (8), δ is the learning algorithm; α is the slope of the neuron.

$\frac{\partial u(c)}{\partial O_l^3(c)}$ is calculated, and equation (9) shows its calculation expression.

$$\begin{cases} \dfrac{\partial u(c)}{\partial O_0^3} = \tau(c) - \tau(c-1) \\ \dfrac{\partial u(c)}{\partial O_1^3(c)} = \tau(c) \\ \dfrac{\partial u(c)}{\partial O_2^3(c)} = \tau(c) - 2\tau(c-1) + \tau(c-1) \end{cases} \tag{9}$$

The calculation equation for adjusting the weight of the HL is shown in equation (10).

$$\begin{cases} \Delta w_{ij}^2(c+1) = \eta^2 \delta^2 O_j^1(c) + \alpha w_{ij}^2(c) \\ \delta_i^2 = g'[net_i^2(k)] \sum_{l=0}^{2} \delta_l^2 w_{ij}^3(c) \\ i = 0,1,2,\ldots,O \end{cases} \tag{10}$$

Thus, an adaptive control algorithm based on improved BP can be obtained, and Fig. 4 shows the algorithm flow.

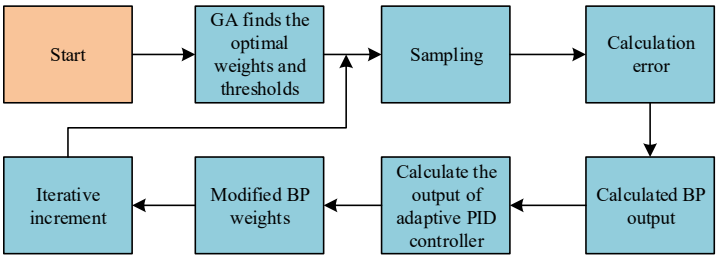

Fig. 4 Flow Chart of Adaptive Control Algorithm Based on Improved BP

In Fig. 4, the initialization operation first sets the optimal weights and thresholds through GA, and the adaptive learning algorithm is set, with the initial iteration times also set. Secondly, by collecting samples to obtain input and OV, the error value at that moment is calculated. Next, the output and input values are calculated, and the obtained OV are the U_D, U_I, and U_p adjustment parameters of the PID controller, and the OV of the adaptive PID controller are calculated. Then, the weights are controlled and adjusted online to achieve the goal of PID adaptive control. Finally, this study will combine improved BP, adaptive PID, SRM, and sensorless to construct an adaptive PID with improved BP and sensorless SRM, as shown in Fig. 5.

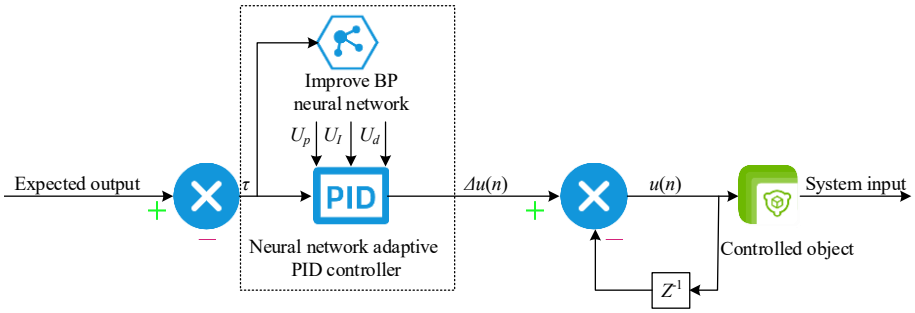

Fig. 5 Adaptive PID Control System Based on Modified BP with Positional Sensorless SRM

In Fig. 5, the system is a closed-loop control that adjusts PID parameters adaptively through BP according to the operating state of the SRM, so that the weight and threshold of the system output and the expected output reach the minimum, thereby achieving the expected control effect. In addition, $\Delta u(n)$ and $u(n)$ in Fig. 5 represent the optimal control increment and optimal control quantity, while Z^{-1} is the parameter.

3. Results

3.1 Performance Analysis of Algorithms

To verify the superiority of the improved BP (Algorithm 1), it was experimentally compared with PSO-BP algorithm (Algorithm 2), Adaptive Network Based Fuzzy Inference System (ANFIS) algorithm (Algorithm 3), and RBF-RLS algorithm (Algorithm 4) in Matlab simulation software. Experimental indicators included fitness and accuracy. Table 1 shows the specific experimental environment.

Table 1

Specific experimental environment of this study

Parameter names	Parameter
Processor	Intel Core i9-13900K
Main frequency	5.8Hz
Internal memory	32GB
Hard disk capacity	500GB
Operating system	Windows 10 64
Matlab version	Matlab 2022a
Data analysis software	Spss26.0

In the above environment, first, a comparative experiment was conducted on the accuracy and loss values of the four algorithms, as shown in Fig. 6.

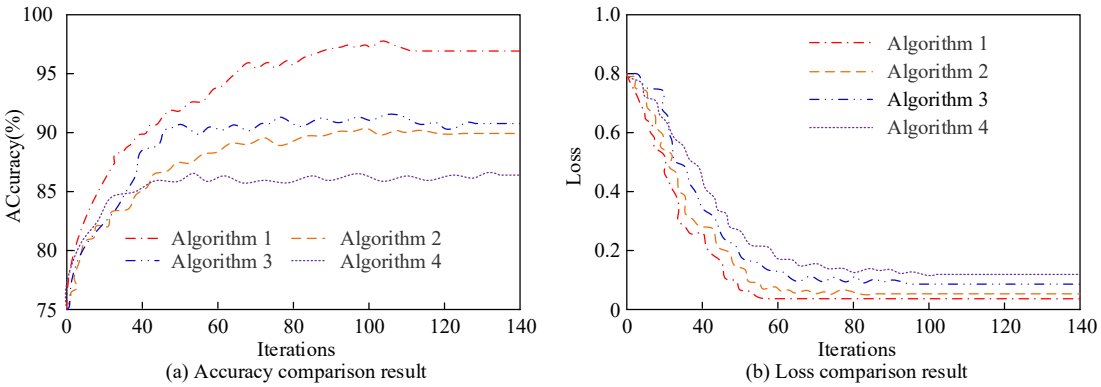

(a) Accuracy comparison result (b) Loss comparison result

Fig. 6 Loss and accuracy Curves for Each Algorithm

In Fig. 6 (a), the average accuracy of Algorithm 1, Algorithm 2, Algorithm 3, and Algorithm 4 were 97.9%, 90.4%, 93.6%, and 86.7%, respectively, with Algorithm 1 having the highest average accuracy. In Fig. 6 (b), the loss curve of Algorithm 1 began to converge at iteration 58, with an average loss value of 0.03, which was lower than Algorithm 2's 0.04, Algorithm 3's 0.08, and Algorithm 4's 0.17. The above results indicated that Algorithm 1 outperformed the compared algorithms in terms of both quasi average accuracy and loss value. The fitness curves and running time comparison results of each algorithm are shown in Fig. 7.

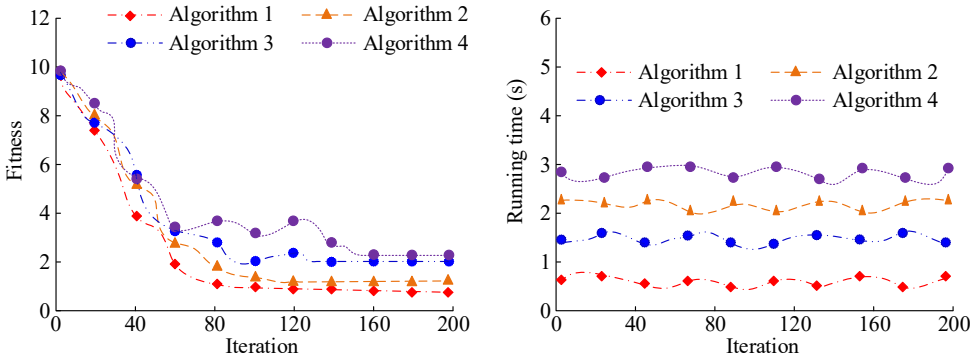

(a) Fitness curves of each method (b) The running time of each method is compared

Fig. 7 Fitness Curve and the Run Time Comparison Results of the Algorithms

In Fig. 7 (a), the fitness curves of Algorithm 1, Algorithm 2, Algorithm 3, and Algorithm 4 began to converge around the 83rd, 121st, 128th, and 158th generations, respectively, with Algorithm 1's fitness curve converging first. In Fig. 7 (b), the average running time of Algorithm 1 was 0.79 seconds, Algorithm 2 was 2.13 seconds, Algorithm 3 was 1.37 seconds, and Algorithm 4 was 2.91 seconds. Among them, Algorithm 1 had the shortest average running time. From the dimensions of runtime and fitness, Algorithm 1 performed best. The fitting results of each algorithm are shown in Fig. 8.

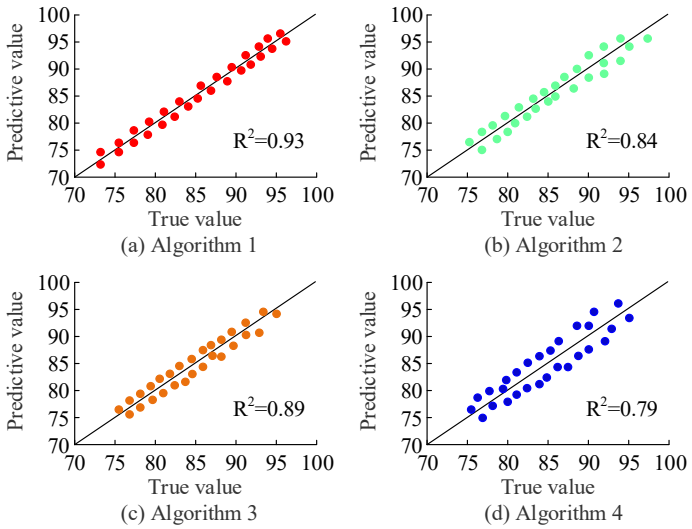

Fig. 8 Results of Fit Degree of Each Algorithm

In Fig. 8, R^2 is the coefficient of fit. The fitting coefficient is a statistical indicator used to measure the degree to which a model fits the data. The closer its value is to 1, the better the fitting effect of the model on the data is, that is, the independent variable can better explain the changes of the dependent variable. Conversely, the closer the R^2 value is to 0, the worse the fitting effect of the model is. In Fig. 8 (a), Algorithm 1 had the most concentrated scatter points, with a fitting coefficient of 0.93. In Fig. 8 (b), Algorithm 2 had scattered points with a fitting coefficient of 0.84. In Fig. 8 (c), the scatter points of Algorithm 3 were relatively concentrated, with a fitting coefficient of 0.89. In Fig. 8 (d), the scatter of Algorithm 4 was the most scattered, with a fitting coefficient of 0.79. From the perspective of fit dimension, Algorithm 1 performed better than the comparison algorithms. Based on the above results, from the dimensions of fitting degree, fitness, accuracy, running time, and loss value, Algorithm 1 had significantly better performance than the compared algorithms and was effective.

3.2 Performance Analysis of Adaptive PID Control System

This study compared the performance the proposed model (System 1), an adaptive PID control system based on PSO-BP sensorless SRM (System 2), an adaptive PID control system based on ANFIS sensorless SRM (System 3), and an adaptive PID control system based on RBF-RLS sensorless SRM (System 4). The comparative indicators included motor response speed, load torque, and rotor angle estimation error. The comparison results of the motor response speed of each system before and after external interference are shown in Fig. 9.

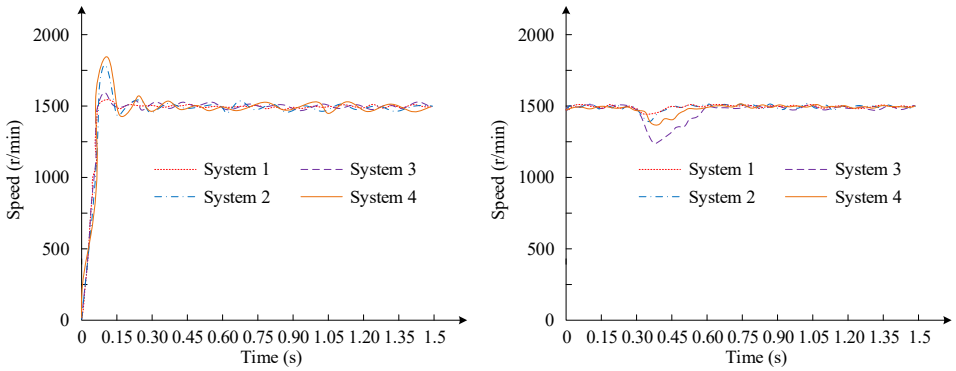

(a) Comparison results of motor speed response of each system

(b) Comparison result of motor speed response of each system when external disturbance is added

Fig. 9 Comparison Results of Motor Speed Response of Each System Before and After External Disturbance

In Fig. 9 (a), when no external interference was added, the motor speed response of System 1 was the fastest, with the smallest overshoot, and the speed was the smoothest after startup. The motor speed response curve of System 2 quickly reached around 1753 revolutions per minute at 0.12 seconds, and then rapidly dropped and stabilized at 1500 revolutions per minute after 0.15 seconds, indicating poor stability. The motor speed response curve of System 3 reached 1570 revolutions per minute at 0.13s, and began to stabilize after 0.15s, reaching 1500 revolutions per minute, which was relatively stable. System 4 had the worst stability, reaching 1768 revolutions per minute at 0.14s, dropping to around 1490 revolutions per minute at 1.5 s, and then stabilizing at 1500 revolutions per minute. In Fig. 9 (b), when external interference was added, System 1 quickly adjusted its own motor speed and had the best stability. Its adaptive dynamic adjustment performance was higher than System 2, System 3, and System 4. From the perspective of motor response speed, System 1 performed better than the comparative system, with good adaptability and robustness. The comparison results of rotor angle estimation error and load torque for each system are shown in Fig. 10.

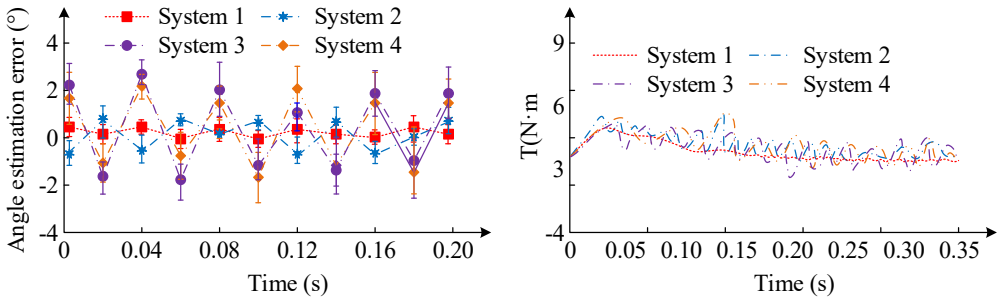

(a) Comparison results of rotor Angle estimation error of each system

(a) Comparison of load torque of each system

Fig. 10. The System Load Torque and Rotor Comparison Estimation Error

In Fig. 10 (a), the fluctuation range of the rotor angle estimation error of System 1 was the smallest, which was smaller than other systems, indicating that the motor can perform steering operation within a certain accuracy. In Fig. 10 (b), the load torque fluctuation of System 1 was the smallest, the load torque of System 2 was larger than that of System 1, the fluctuation of System 3 was higher than that of System 2, and the fluctuation of System 4 was the largest. From the perspective of rotor estimation error and load torque, compared to the comparative system, System 1 had the best performance. From the perspective of rotor angle estimation error, load torque, and motor speed response dimensions, System 1 performed the best, indicating the feasibility of the sensorless SRM adaptive control algorithm.

4. Discussion

This study compared and analyzed the performance of improved BP and an adaptive PID with improved BP for sensorless SRM. Improved BP algorithm had significant advantages in terms of running time, accuracy, and loss value. In the accuracy comparison experiment, the average accuracy of the improved BP, PSO-BP, ANFIS, and RBF-RLS algorithms were 97.9%, 90.4%, 93.6%, and 86.7%, respectively, with the proposed improved BP algorithm having the highest average accuracy. This indicated that the introduction of GA algorithm optimized the algorithm's ability to find the optimal solution and improved its performance from the perspective of accuracy. This result was in line with the improved BP algorithm suggested by Zhu J et al. [17]. In the loss value comparison experiment, the average loss values of the improved BP, PSO-BP, ANFIS, and RBF-RLS algorithms were 0.03, 0.04, 0.08, and 0.17, respectively. Among them, the improved BP algorithm had the lowest loss rate, indicating that the introduction of adaptive learning rate algorithm and additional momentum algorithm improved the algorithm performance and enhanced the computing power of BP. Meanwhile, in the comparison experiment of running time and fitting degree, the fitting coefficient and average running time of the proposed model were 0.93 and 0.79 seconds, respectively. This result indicated that the performance of the improved BP was significantly improved, further verifying the superiority. Kumar R reached similar conclusions in his research on improving the BP algorithm [18]. Secondly, in the comparative analysis of the performance of adaptive PID control systems, the proposed system showed good performance in terms of rotor angle estimation error, load torque, and motor speed response dimensions. In terms of motor speed response, compared to the comparative system, this system had the best performance, with good adaptability and robustness. In terms of load torque and rotor angle estimation errors, this system had the smallest error estimation and the smallest load torque fluctuation, both of which were superior to the comparison system. This result indicated that the introduction of adaptive learning algorithm,

additional momentum algorithm, and GA improved the performance of the system, resulting in good control effect. This conclusion is aligned with the findings from relevant studies conducted by Kaveh M and Mesgari M.S. in 2023 [19]. This result indicated that the adaptive PID control system based on improved BP for sensorless SRM could effectively enhance the reliability of SRM system operation and reduce costs.

5. Conclusion

In view of the current problem of low accuracy in SRM control using sensorless methods, the research introduced adaptive learning rate algorithm, additional momentum term algorithm, and GA to improve BP. Moreover, an adaptive PID with improved BP for sensorless SRM is constructed. Through comparative analysis of algorithms, it was found that the improved BP performed significantly the best in terms of running time, loss value, accuracy, and fitting degree. Subsequently, the adaptive PID control system of sensorless SRM based on improved BP were compared and analyzed with other systems in terms of load torque, motor speed response, and rotor angle estimation error dimensions. Compared with the comparison system, the proposed system had the best performance. The above results indicated that the improved BP algorithm proposed in the study has strong adaptability and robustness. The limitation of this study is that it did not consider the noise of SRMs, and noise constraints are a further direction for research.

REFERENCES

[1] *Sun X, Zhu Y, Cai Y, Xiong, Y., Yao, M., Yuan, C.* Current fault tolerance control strategy for 3-phase switched reluctance motor combined with position signal reconstruction. IEEE Transactions on Energy Conversion, Vol. **38,** Iss. 3, 2023.

[2] *Ananda Padmanaban L, Saravanan P.* Design, analysis and comparison of switched reluctance motors for electric vehicle application. Automatika: časopis za automatiku, mjerenje, elektroniku, računarstvo i komunikacije, Vol. **64,** Iss. 2, 2023.

[3] *Feng L, Sun X, Yang Z, Diao, K.* Optimal torque sharing function control for switched reluctance motors based on active disturbance rejection controller. IEEE/ASME Transactions on Mechatronics, Vol. **28**, Iss. 5, 2023.

[4] *Dejamkhooy A, Ahmadpour A.* Torque ripple reduction of the position sensor-less switched reluctance motors applied in the electrical vehicles. Journal of Operation and Automation in Power Engineering, Vol. **11**, Iss. 4, 2023.

[5] *Fang C, Chen H, Wang X, Zhang, J., Li, Y., Torkaman, H.* Current estimation of switched reluctance motor based on piecewise model and iteration calculation. International Journal of Circuit Theory and Applications, Vol. **51,** Iss. 4, 2023.

[6] *Sun X, Xiong Y, Yao M, Wu, J.* High fault-tolerance evaluation on position signal for switched reluctance motor drives. IEEE Transactions on Energy Conversion, Vol. **37**, Iss. 3, 2022.

[7] *Kumar M N, Chidanandappa R.* Particle swarm optimization technique for speed control and torque ripple minimization of switched reluctance motor using PID and FOPID controllers. International Journal of Information Technology, Vol. **16,** Iss. 2, 2024.
[8] *Jing B, Dang X, Liu Z, Wang, J, Jiang, Y.* Torque Ripple Reduction Of Switched Reluctance Motor Based On Neural Network Sliding Mode Parameter Online Learning. Journal of Applied Science and Engineering, Vol. **27**, Iss. 6, 2024.
[9] *Yang E, Pan J, Wang X, Yu, H., Shen, L., Chen, X.* Adatask: A task-aware adaptive learning rate approach to multi-task learning. Proceedings of the AAAI conference on artificial intelligence. Vol. **37**, Iss. 9, 2023.
[10] *Li C, Jia T, Han X, Jiang, X.* Study on parameter optimization of laser cladding Fe60 based on GA-BP neural network. Journal of Adhesion Science and Technology, Vol. **37**, Iss. 18, 2023.
[11] *Shen W, Li G, Wei X, Fu, Q., Zhang, Y., Qu, T.* Assessment of dairy cow feed intake based on BP neural network with polynomial decay learning rate. Information Processing in Agriculture, Vol. **9**, Iss. 2, 2022.
[12] *Zhou D, Chen H, Wang X, Pires, V. F., Martins, J.* Synthetic sensorless control scheme for full-speed range of switched reluctance machine drives with fault-tolerant capability. IEEE Transactions on Transportation Electrification, Vol. **8**, Iss. 4, 2022.
[13] *Choudhuri S, Adeniye S, Sen A.* Distribution Alignment Using Complement Entropy Objective and Adaptive Consensus-Based Label Refinement For Partial Domain Adaptation. Artificial Intelligence and Applications. Vol. **1**, Iss. 1, 2023.
[14] *Zhao J, Yan H, Huang L.* A joint method of spatial–spectral features and BP neural network for hyperspectral image classification. The Egyptian Journal of Remote Sensing and Space Science, Vol. **26**, Iss. 1, 2023.
[15] *Wang D, Luo H, Grunder O, Lin, Y., Guo, H.* Multi-step ahead electricity price forecasting using a hybrid model based on two-layer decomposition technique and BP neural network optimized by firefly algorithm. Applied Energy, Vol. **190**, Iss. 3,2017.
[16] *Doerr B, Echarghaoui A, Jamal M, Krejca, M. S.* Runtime Analysis of the (μ+ 1) GA: Provable Speed-Ups from Strong Drift towards Diverse Populations, Proceedings of the AAAI Conference on Artificial Intelligence. Vol. **38**, Iss. 18, 2024.
[17] *Zhu J, Zheng H, Yang L, L., Li, S., Sun, L., Geng, J.* Evaluation of deep coal and gas outburst based on RS-GA-BP. Natural Hazards, Vol. **115**, Iss. 3, 2023.
[18] *Kumar R.* Double internal loop higher-order recurrent neural network-based adaptive control of the nonlinear dynamical system. Soft Computing, Vol. **27**, Iss. 22, 2023.
[19] *Kaveh M, Mesgari M S.* Application of meta-heuristic algorithms for training neural networks and deep learning architectures: A comprehensive review. Neural Processing Letters, Vol. **55**, Iss. 4, 2023.